

# Toxicology Research

Accepted Manuscript



This is an *Accepted Manuscript*, which has been through the Royal Society of Chemistry peer review process and has been accepted for publication.

*Accepted Manuscripts* are published online shortly after acceptance, before technical editing, formatting and proof reading. Using this free service, authors can make their results available to the community, in citable form, before we publish the edited article. We will replace this *Accepted Manuscript* with the edited and formatted *Advance Article* as soon as it is available.

You can find more information about *Accepted Manuscripts* in the [Information for Authors](#).

Please note that technical editing may introduce minor changes to the text and/or graphics, which may alter content. The journal's standard [Terms & Conditions](#) and the [Ethical guidelines](#) still apply. In no event shall the Royal Society of Chemistry be held responsible for any errors or omissions in this *Accepted Manuscript* or any consequences arising from the use of any information it contains.

## ARTICLE

## Label-free Monitoring of the Nanoparticle Surface Modification Effects on Cellular Uptake, Trafficking and Toxicity

Cite this: DOI: 10.1039/x0xx00000x

D. Bartczak<sup>a</sup>, M.-O. Baradez<sup>a</sup>, H. Goenaga-Infante<sup>a</sup> and D. Marshall<sup>a\*</sup>Received 00th January 2012,  
Accepted 00th January 2012

DOI: 10.1039/x0xx00000x

www.rsc.org/

Changing the surface functionality of nanoparticles (NP) through the addition of organic ligands and/or biomolecules is a common approach to reduce their potential toxicity. However, understanding how the surface modifications change NP's mechanism of action and behaviour in the presence of biological matrix is a complex challenge. It is often exacerbated by necessary sample pre-processing, which may alter NP characteristics limiting provided information, yet is required by majority of available physicochemical characterisation techniques. In this study we have adopted label-free kinetic measurements of NP size, charge and toxicity performed in biological matrix *in situ* to demonstrate how careful engineering of the NP surface dramatically changes their toxicity profiles, due to the rate the particles are taken up by cells. We also show how NP capping with proteins alters their cellular uptake pathway as well as intracellular trafficking and that endosomes acidification is an important cell defence mechanism. The results presented in this study, supported by other commonly used techniques, highlights a synergy between NP surface chemistry and their bioactivity, which could be used to influence development of safer nano-enabled products.

### Introduction

The unique physicochemical properties of nano-structured materials are leading to their increased application in everyday commercial products. For example, zinc oxide (ZnO) nanoparticles (NP) have a high refractiveness<sup>1</sup> and a broad absorption band in the UV region<sup>2</sup> resulting in their widespread use in sunscreens, cosmetics and paints, whilst their increased chemical reactivity<sup>3</sup> provides benefits for their use in catalysis and chemical sensing. ZnO NP also display semiconductor properties with a band gap at  $\sim 3.3\text{eV}$ <sup>4</sup>, making them a popular candidate for development of solar cells, excitonic lasers as well as luminescent and piezoelectric devices. Despite their widespread applications, there is potential for NP to become released from products during their natural lifecycle, thereby posing a risk of human exposure.<sup>5</sup> This has raised concerns over possible toxicity of NP if they are ingested, inhaled or absorbed through the skin or if NP undergo functional changes following exposure through interactions with biological fluids.

Due to potentially adverse effects of NP on human and the environment, current research efforts are focused on the development of their less toxic and more biocompatible

versions<sup>6</sup>, a concept known as 'safe by design'. One popular way to achieve this is to modify the NP surface with organic ligands, like silane derivatives and biomolecules or to dope with less toxic inorganic components, such as iron oxide.<sup>7</sup> Carefully chosen ligands or dopants form an outer layer encapsulating the ZnO core, which prevents direct contact with the surrounding environment, leading to substantial reduction in the toxicity of the materials and preventing degradation, thus the NP properties can be retained for longer.

Verification of the ligands (or dopants) suitability and the resulting changes in NP toxicity is typically performed using *in vitro* cellular screens in a defined biological media, often containing serum proteins. These systems not only support the growth of the cells but also mimic the corporeal environment that NP are likely to encounter following human exposure. However, while the biological media is good for supporting cell proliferation it presents a challenging environment in which to characterise the types of physical and chemical changes that NP may undergo.<sup>8</sup> There are also many difficulties associated with the adaptation of traditional *in vitro* assays for toxicological assessments of metal and metal oxide NP. In particular, possible interferences of NP with soluble indicators used in

viability assays<sup>9</sup>, due to the luminescent and semiconductor properties of NP, often enhance or quench the test signal leading to false positive or negative readouts.

A number of reports have highlighted the need to develop reliable strategies to measure the physical and chemical changes that NP undergo when they encounter biological matrices and link these changes to their potential toxicity.<sup>8,10</sup> This is a complex task requiring a combination of NP characterisation techniques and toxicological screening approaches. In this study we use a multi-platform approach to characterise the physicochemical and extrinsic changes that ZnO NP capped with an array of surface ligands undergo in a defined serum containing biological media (*in situ*) in a time dependent manner, demonstrating both the extent and rate over which exchange/capping reactions occur. We also demonstrate how different capping ligands affect the toxicity of ZnO NP in the HepG2 cell model using impedance spectroscopy based real-time cell electronic sensing (RT-CES) which is known to overcome the limitations of traditional viability screens<sup>11</sup>. ZnO NP were selected for this study since the materials toxicity is well studied and it has numerous commercial applications which use surface functionality to potentially reduce toxicity. The HepG2 model was selected as it is a model of the liver which is a major site for bioaccumulation of NP following exposure, irrespective of their entry route into the body. Using this approach we demonstrate how the presence of proteins on the NP surface triggers the activation of different NP uptake mechanisms. Taken together these results show how surface modifications influence NP interactions with biological matrices, their cellular uptake, cellular trafficking and ultimately their toxicity, providing a platform for assessing their overall safety.

## Experimental

**Preparation of plain and capped ZnO NP.** Commercially available zinc oxide nanopowder (10-30nm, US Research Nanomaterials) was dispersed in water or capped with a selection of ligands using previously described protocol.<sup>12</sup> Briefly, 5mg of powder was sonicated for 15min. at room temperature (plain, APTMS and APTMS-BSA) or at 4<sup>0</sup>C (BSA, in order to avoid protein denaturation) in the ultrasonic bath (power 150W) with 50 $\mu$ l of isopropanol. Next, 5ml of ultrapure water (plain), 5ml of 2% 3-aminopropyltrimethoxysilane (APTMS) in isopropanol (APTMS and APTMS-BSA) or 5ml of 0.05% bovine serum albumin fraction V in ultrapure water (BSA) was introduced and the suspension was sonicated for 1h at room temperature (plain, APTMS and APTMS-BSA) or with a gradual temperature increase to room temperature (BSA). NP were then reacted for additional 24h at room temperature (plain and BSA) or at 60<sup>0</sup>C (APTMS and APTMS-BSA) with shaking, prior to purification from excess ligands and/or organic solvent residues by triple centrifugation/decantation (13'000rpm, 15min., room temperature). Capped NP were redispersed by sonication in ultrapure water at 5mg/ml. BSA was covalently

conjugated to APTMS capped NP (APTMS-BSA) using EDC/sulfo-NHS coupling agents. Briefly, 0.34mg of APTMS capped NP was redispersed by sonication in 5ml of 0.01M borate buffer pH9. Then, 100 $\mu$ l of BSA fraction V stock (1mM in ultrapure water), 50 $\mu$ l of EDC (0.198M in ultrapure water) and 100 $\mu$ l of sulfo-NHS (0.198M in ultrapure water) were introduced. After, 48h stirring at room temperature, the conjugates were purified by triple centrifugation/decantation (13'000rpm, 15min., room temperature) and redispersed by sonication in ultrapure water or cell culture media at 5mg/ml.

### Sizing and zeta-potential characterisation in solution.

Suspensions of NP (30-70  $\mu$ g/ml) were prepared in ultrapure water or cell culture media (EMEM 10% FBS) by sonication. The movement of NP in suspensions under Brownian motion (sizing) or under applied electrical current (zeta-potential) was recorded with NanoSight NS500 over 15-90 sec. The influence of cell culture media on NP was studied over 0-24h time course, at 37<sup>0</sup>C and room temperature. Recorded movies were analysed with NTA 2.2 software using detection threshold value 9 and a minimum expected particle size of 30nm. All experiments were performed in triplicates using different batches of NP and are presented as average  $\pm$  standard deviation.

**Organic corona quantification.** NP surface coverage with ligands was quantified with a colorimetric assay (FluoroProfile, Sigma-Aldrich), based on individually prepared standard curves. The assay was performed according to the manufacturer protocol in a 96-well format (high quality flat bottom black microplates; Sigma-Aldrich). The fluorescence intensity at 620nm was recorded with 510nm excitation wavelength and Tecan Infinite M200 plate reader. Estimated empirical number of ligands and theoretically calculated number of NP in the sample (based on the size values obtained with NTA; see ESI) gave the average number of ligands per NP. All experiments were performed in triplicates using different batches of NP and are presented as average  $\pm$  standard deviation.

**TEM imaging.** 10 $\mu$ l of NP suspension (0.5mg/ml) was deposited on a TEM grid (carbon film on 400 mesh Cu, Agar Scientific) and air dried. TEM grids were imaged with an Hitachi H7000 transmission electron microscope operating at 75kV voltage with 100,000x magnification (Biomedical Imaging Unit, Southampton, UK).

**NP dissolution rate.** NP suspensions were incubated in water or cell culture media (30-70 $\mu$ g/ml) for 24h at 24 or 37<sup>0</sup>C respectively, and then centrifuged at 13'000rpm for 15min. Collected supernatants (dissolved ions) as well as the whole samples (NP plus dissolved ions) were mineralised using a microwave (Milestone, equipped with SK10 rotor) by supported digestion in 1:1 nitric acid and hydrogen peroxide and analysed for the <sup>66</sup>Zn <sup>68</sup>Zn content with an Agilent 7700x spectrometer, operating in a He mode. All experiments were

performed in triplicates using different batches of NP and are presented as average  $\pm$  standard deviation.

**Dose response to NP.** HepG2 cells (passage 80-83, LGC Standards UK) were seeded directly in a standard E-Plate (96-well, Roche Diagnostics) at a density of 20,000cells/well and grown in 200 $\mu$ l EMEM supplemented with 10% FBS, PAA Laboratories for 24h in an air balanced incubator (5% CO<sub>2</sub>, 37°C) with the cell impedance measured every hour using a standard RT-CES instrument (Acea Biosciences). Following the initial 24h after seeding the cells were exposed to various concentrations of NP (10-70 $\mu$ g/ml) suspended in cell culture media, and their biological status was monitored for further 24h with the impedance values recorded every hour.

**NP uptake determination.** HepG2 cells (passage 80-83, LGC Standards) were seeded in a culture dish (24-well microplate, PAA Laboratories) at density of 200,000cells/well. The cells were grown in 1ml EMEM supplemented with 10% FBS for 24h in an air balanced incubator at 5% CO<sub>2</sub>, 37°C. After the initial 24h incubation, cell culture media was removed and freshly prepared NP suspensions were introduced (1ml/well, 30 $\mu$ g/ml). Cells were incubated for a further 4h, washed twice with PBS (0.5ml/well, Sigma-Aldrich), then briefly with trypsin/EDTA solution (0.5 ml/well, Sigma-Aldrich) to remove excess NP weakly associated with cell membrane and harvested with trypsin/EDTA solution for 1h. Collected cell suspensions/lysates were mineralised using acid supported microwave digestion (Milestone, Analytix) and analysed for the total content of <sup>66</sup>Zn and <sup>68</sup>Zn with ICP-MS (Agilent 7700, Postnova) operating in the He mode.

**Inhibition of the NP uptake.** HepG2 cells (passage 80-83, LGC Standards) were seeded directly in a standard E-Plate (96-well, Roche Diagnostics) at the density of 20,000cells/well and grown in 190 $\mu$ l EMEM supplemented with 10% FBS for 24h in an air balanced incubator at 5% CO<sub>2</sub>, 37°C with the impedance measurements taken every hour. Following the initial 24h after seeding, solutions of the following drugs were added to the wells: nocodazole (10 $\mu$ l, 20 $\mu$ M final, Sigma-Aldrich), benzamil (10 $\mu$ l, 50 $\mu$ M final, Sigma-Aldrich), chloroquine (10 $\mu$ l, 100 $\mu$ M final, Sigma-Aldrich) or chlorpromazine (10 $\mu$ l, 15 $\mu$ M final, Sigma-Aldrich) and the cells were incubated for 0.5h with the impedance measured every 5min. Subsequently, media was removed and the cells were exposed to NP suspended in drugs containing cell culture media (200 $\mu$ l, 30 $\mu$ g/ml) for 4h with the impedance measured every 0.5h. After the treatment, NP suspensions were removed and the cells were incubated in fresh cell culture media (200 $\mu$ l) for an additional 20h with the cell impedance measured every hour.

## Results and Discussion

### Surface modification of ZnO NP.

The ZnO NP with a primary crystal size of 10-30nm (as specified by the manufacturer and verified with SEM analysis; **ESI, Fig. S1**) were functionalised with either 3-aminopropyltrimethoxysilane (APTMS), a loosely bound corona of bovine serum albumin proteins (BSA), or with APTMS followed by covalent attachment of BSA using EDC/sulfo-NHS (schematic representation of different surface functionalities is shown in **Figure 1A**). Functionalisation did not affect the semiconductor properties of ZnO NP, whilst only slight shifts in the absorption maxima were observed, due to changes in the refractive index of the surrounding media, as previously reported.<sup>12</sup> The number of ligands attached to the surface of NP (**Figure 1B**) was determined with a fluorescent probe for water suspensions of NP (dark bars) or after 24h incubation in cell culture media containing 10% serum at 37°C (10% FBS EMEM; light bars). These analysis showed that when suspended in water NP capped with small inorganic molecule APTMS had the highest number of ligands attached to their surface, which based on calculations accounts for ~90% surface coverage.<sup>13</sup> NP capped with large proteins (BSA alone or APTMS-BSA) generally had a lower number of ligands on their surfaces, although the NP with loosely bound corona (BSA) had ~4 times more BSA ligands, suggesting the formation of multiple layers. As expected, only background levels of ligands were measured on the surface of plain NP. After 24h in cell culture media, there was ~27-fold increase in the number of ligands attached to the surface of plain NP, as they adsorbed constituents from the media. The number of ligands on the surface of NP capped with APTMS and APTMS-BSA remained stable, while the NP capped with BSA alone underwent an approximately 4-fold reduction in the number of ligands on their surface.

### Characterisation of ZnO NP suspended in serum-containing cell culture media.

To understand how the differently capped NP behave during the *in vitro* testing they were characterised for their physical (hydrodynamic diameter) and extrinsic ( $\zeta$ -potential) properties following suspension in cell culture media over 0-24h time course. NP characterisation within biological matrix, whilst challenging, is essential as it informs on structural and functional changes NP undergo, which in turn could alter the toxicity profile of the material.<sup>14</sup> Changes in the selected NP properties were observed in the real-time using nanoparticle tracking analysis (NTA) platform in the presence of serum proteins and other components of the cell culture media. Size analysis showed that the hydrodynamic diameter of NP suspended in cell culture media changed compared to water suspensions (**Table 1**), and also that the trend NP follow depends on the type of ligand, however the differences between the individual test groups were not significant.

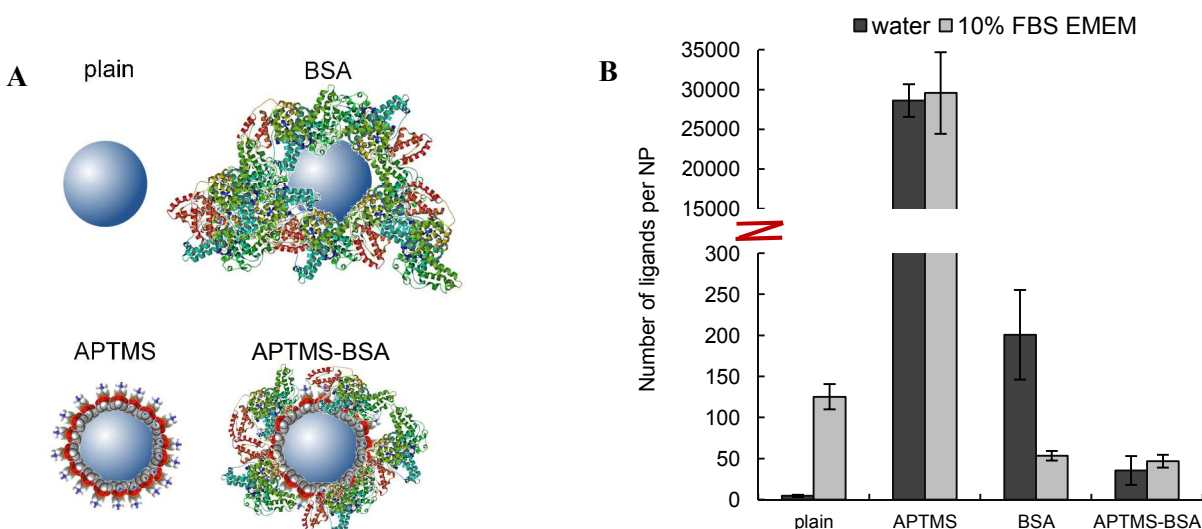


**Figure 1.** Schematic representation of plain and capped ZnO NP (A) and estimated average number of ligands per NP (B; average  $\pm$  stdev,  $n=3$ ).

**Table 1.** Changes in hydrodynamic diameter of ZnO NP in 10% FBS EMEM over 0-24h time course (average  $\pm$  stdev,  $n=3$ ).

NP type	NP diameter [nm] *			
	water	10% FBS EMEM		
		0h	4h	24h
plain	31.0 $\pm$ 0.5	29.0 $\pm$ 2.6	35.7 $\pm$ 3.2	28.0 $\pm$ 2.6
APTMS	31.4 $\pm$ 0.6	34.3 $\pm$ 2.5	31.3 $\pm$ 0.3	34.0 $\pm$ 2.6
BSA	28.7 $\pm$ 2.9	35.3 $\pm$ 2.1	31.7 $\pm$ 0.3	32.7 $\pm$ 0.6
APTMS-BSA	32.3 $\pm$ 0.8	37.9 $\pm$ 2.0	37.7 $\pm$ 2.0	37.3 $\pm$ 3.2

\*diameter was measured *in situ*

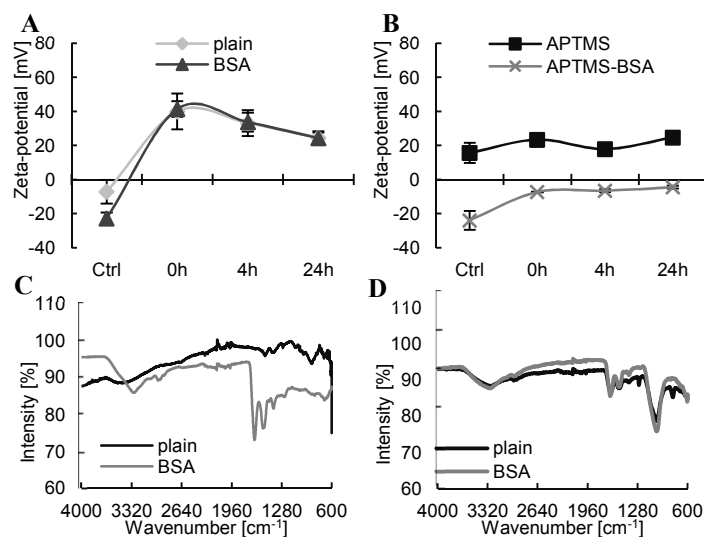


**Figure 2.** Changes in  $\zeta$ -potential of ZnO NP in biological media over 0-24h time course (average  $\pm$  stdev,  $n=3$ ); measured *in situ* (A and B). Representative FTIR spectra of ZnO NP in water (C) and 10% FBS EMEM (D).

Measurements of  $\zeta$ -potential showed that in water ( $\sim$  pH 5.4) plain ZnO NP (Figure 2A, Ctrl) do not possess any significant positive or negative surface charge ( $\zeta$ -potential of  $-7.13 \pm 7.08$ ). In comparison, NP functionalised with APTMS became positively charged (Figure 2B, Ctrl) and NP capped with BSA directly (Figure 2A, Ctrl) or with BSA covalently conjugated to APTMS (APTMS-BSA Figure 2B, Ctrl) became negatively charged. Following suspension in cell culture media (EMEM supplemented with 10% FBS,  $\sim$  pH 7.4), plain and BSA capped NP (Figure 2A) underwent significant changes in their  $\zeta$ -potential within the first 4h, becoming positively charged, likely due to the rapid ligand exchange with components of the cell culture media. Following the initial increase, their charge gradually decreased over the next 20h and eventually stabilised at around 24mV. FTIR spectra (Figure 2D) confirmed the association of media components with these NP, compared to water suspensions (Figure 2C, ESI Fig. S2), and since, culture media used in this study was well defined, containing known quantities of organics, mostly proteins (4.2g/litre; albumin, globulins and haemoglobin) and glucose (1g/litre), it was possible to determine the occurring binding events. FTIR showed a strong peak in the region around  $1070\text{cm}^{-1}$  wavenumber, associated with the C-O stretch in a primary alcohol ( $-\text{CH}_2\text{-OH}$ ), which in this case most likely comes from glucose.<sup>15</sup> The presence of glucose on the surface of the NP is of particular interest, since other studies have shown it can increase NP uptake by  $>30\%$  and have further implications on the cellular response.<sup>16</sup> FTIR also showed peaks at  $1600\text{-}1690\text{cm}^{-1}$  and  $1480\text{-}1575\text{cm}^{-1}$ , which are typical features of amide I and amide II respectively and therefore correspond to binding of proteins. Among proteins associated with the NP, predominantly haemoglobin and albumin were identified (from tryptic digests, using Agilent nanoLC-QToF mass spectrometer and the Mascot data base; data not shown). The presence of haemoglobin explains the observed changes in zeta-potential values of the NP in cell culture media. Haemoglobin is

positively charged in the media (calculated PI is 9.84, whilst cell culture media pH is 7.4) and as it sorbes onto the negatively charged BSA NP (calculated PI value for BSI is 5.71) it causes a rise in the zeta-potential values, until an equilibrium is reached. In comparison, the NP capped with APTMS or APTMS-BSA (**Figure 2B**) had no significant change in surface charge when suspended in cell culture media and both retained their original charge status throughout the test period. It is worth noting that after 24h in cell culture media APTMS-BSA NP were the only type of test NP remaining negatively charged, whilst the other three types of NP (plain, BSA and APTMS capped) showed relatively similar  $\zeta$ -potential of around 24mV (**Figure 2A and 2B**).

More traditional techniques like ICP-MS and TEM, involving sample pre-processing before analysis, were adopted to assess the structural changes NP undergo in cell culture media, such as their dissolution rate (**Figure 3A**). Following functionalisation, all types of NP were relatively stable, with a dissolution levels <5% when suspended in water (dark grey bars).

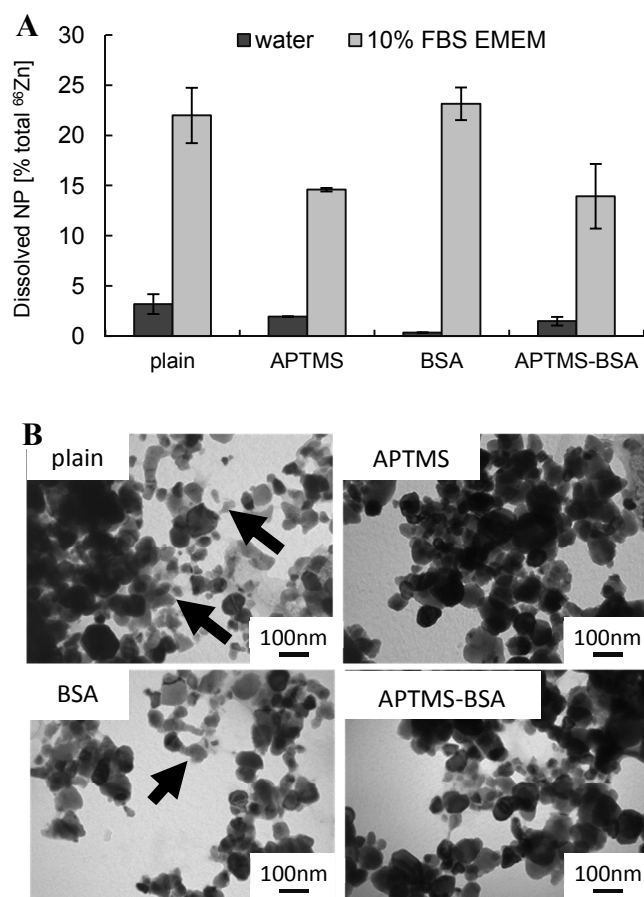


**Figure 3.** Dissolution rate of ZnO NP in water and 10% FBS EMEM (**A**; average  $\pm$  stdev,  $n=3$ ), determined after 24h incubation. Representative TEM images of ZnO NP after 24h incubation in 10% FBS EMEM (**B**); arrows indicate decomposed NP.

However, after 24h incubation in cell culture media (light grey bars) the percentage of dissolved Zn fraction increased,

with higher dissolution levels (>20%) for plain and BSA capped NP and significantly lower dissolution rate (~14%) for APTMS and APTMS-BSA samples, suggesting that functionalisation with APTMS prevents direct contact with the surrounding media and offers the inner core some level of protection. The degradation of NP in cell culture media can also be seen on TEM images (**Figure 3B**, arrows). Decomposed NP appeared smaller with sharper edges and irregular shape, as opposed to other near-spherical objects. Areas with NP of uneven or checkered contrast indicate inner disintegration. Overall, higher content of decomposed NP were found on TEM images for plain and BSA NP, than APTMS and APTMS-BSA NP, in line with the ICP-MS dissolution data. No clear shape variation between NP with different functionality was noted. Particles displayed on the TEM micrographs formed larger agglomerates and/or aggregates, which was attributed to an artefact arising from the sample preparation (air drying), since the size as well as  $\zeta$ -potential distributions in suspension (**ESI, Fig. S3**) indicated well dispersed materials.

### Toxicity of ZnO to HepG2.

Human liver cell model (HepG2) was employed to examine the effects of NP surface functionality as well as subsequent changes in physicochemical and extrinsic profiles (following incubation in cell culture media) on their biological activity. Toxicity levels of NP after 24h treatment over a concentration range between 10 $\mu$ g/ml and 70 $\mu$ g/ml are shown in **Figure 4A**. Toxicity was determined using label free impedance spectroscopy and is shown as a percentage of total cell number as there is a direct linear correlation between impedance measurement and cell number (**ESI, Fig 4**).

The response of HepG2 to ZnO NP was dose dependent with similar  $EC_{50}$  values observed for plain, APTMS and BSA NP at 37.3 $\mu$ g/ml, 33.1 $\mu$ g/ml and 29.4 $\mu$ g/ml, respectively. In comparison, APTMS-BSA NP were much less toxic to HepG2 with an  $EC_{50}$  value of 62.7 $\mu$ g/ml. This difference in the observed toxicity is likely due to the negative charge exhibited by APTMS-BSA NP, which could cause them to be slightly repelled from the negatively charged surface of the cells, lowering the number of particles directly interacting with the cells and thereby reducing the toxic response. A similar response has been reported for anionic NP, which have much lower toxicity than their neutral or anionic forms and elicit differential mechanisms of cell death.<sup>17</sup> Furthermore, no toxicity was measured in the HepG2 cell model when exposed to the capping ligand alone or non-toxic NP such as TiO<sub>2</sub> capped with the same ligands (**ESI, Fig. S5**) indicating that the observed toxicity is not due to microbial or chemical contamination introduced during NP processing.

To investigate if the toxicity profiles correlate with the effect of NP on cell behaviour, kinetic responses of cells to NP at a concentration of 30 $\mu$ g/ml were examined (**Figure 4B**). The selected concentration correlates with the approximate  $EC_{50}$  values for plain, APTMS and BSA capped NP. These analyses

showed that plain NP instigated a strong cellular response, indicated by a rapid increase in the impedance values, sustained for ~16h and peaking twice, with a stronger secondary response after 8h of treatment. This was followed by a development of mild cellular toxicity and a reduction in viability to 85%. NP capped with APTMS induced a weaker cellular response that lasted for ~6h, although they induced stronger toxicity, reducing cell viability to 65% after 24h. The lowest cellular response occurred in the presence of BSA NP and lasted for only 3h, followed by a strong toxic response reducing cell viability to 47% after 24h. The NP capped with APTMS-BSA induced a cellular response comparable to the NP capped with APTMS alone but had no significant toxic effect on the cells, with viability stabilising at 94% after 16h. Previous studies looking at the toxicity of ZnO NP in other cell lines such as the A549 respiratory model have shown similar toxicity and demonstrated that this initial response is linked to uptake and subsequent extrusion of NP by cells before the onset of apoptosis<sup>11</sup>. In this study we show a reversely proportional correlation between the strength of this initial cellular response (i.e. NP extrusion) and the NP toxicity, with less toxic particles such as the plain or APTMS-BSA NP inducing a stronger response than the more toxic BSA and APTMS capped NP. It is also interesting to note that the negatively charged APTMS-BSA capped NP have not triggered a cell response until 4h after exposure, compared to 2h for the other NP, further suggesting that they may be repelled from the surface of the negatively charged cells reducing NP-cell contact and subsequent toxicity.

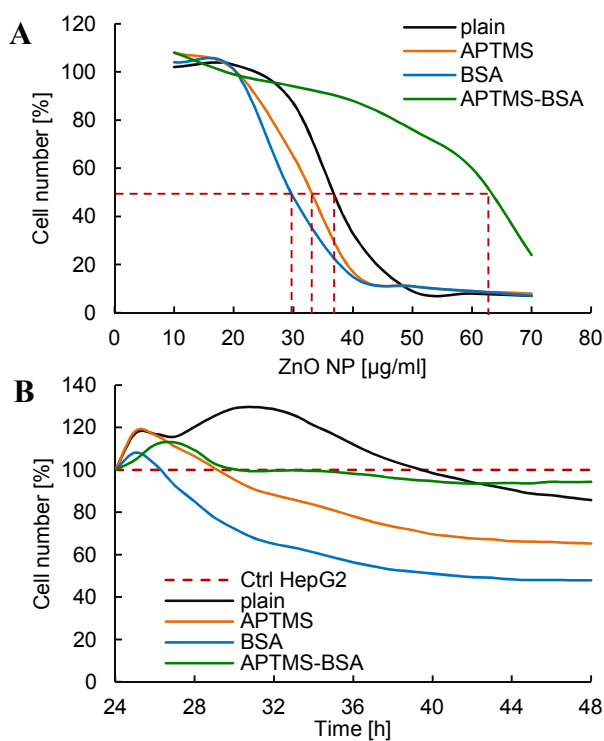


**Figure 4.** Determined with impedance sensing cytotoxicity of ZnO NP administrated at a dose range 10-70µg/ml (A); EC<sub>50</sub> values marked in red. HepG2 response to ZnO NP at 30µg/ml (B); normalized to untreated cells (Ctrl HepG2, marked in red).

**Table 2.** Uptake rate of ZnO NP by HepG2 and corresponding intercellular levels of ROS (n=3), determined after 4h treatment.

NP type	Uptaken NP [% introduced <sup>66</sup> Zn]		ROS production [% increase]	
	Average	Stdev	Average	Stdev
plain	0.08	0.01	8.03	1.39
APTMS	1.02	0.01	8.89	3.09
BSA	0.86	0.04	10.14	3.58
APTMS-BSA	0.15	0.01	11.24	4.00

#### ZnO NP uptake rate and internalisation route.

It is often speculated whether NP-cell contact is sufficient for the activation of a cytotoxic response or if cellular uptake is required.<sup>18</sup> To investigate this we have determined the level of internalised NP with ICP-MS, whilst their effect on cells was measured through the production of reactive oxygen species (ROS, Table 2).

The production of ROS is often used as a key marker in the assessment of NP toxicity, because it acts as a trigger for secondary processes such as the production of proinflammatory cytokines and other signalling molecules, representing all stages in the hierarchical oxidative stress model and ultimately leading to cell damage and death.<sup>18</sup> In all cases the uptake of the NP was associated with an increase in ROS with an average increase across all the NP types of  $9.6 \pm 3.0\%$  compared to untreated controls. Similar levels of ROS suggest that the observed toxic effects are linked with the NP direct interaction with cells (i.e. NP uptake) and not with the release of ions into the surrounding media due to the NP dissolution, which has varied significantly between the tested types of NP's surface ligands.

For all tested materials, the amount of internalised NP was below 1.5% of the introduced quantity, indicating that the administrated dose of NP was in excess, hence, their uptake rates were not controlled or limited by the number of NP available to cells. The uptake rates of NP with different surface functionalities varied significantly, with plain and APTMS-BSA NP taken up in relatively low numbers (<0.2% of initial NP concentration) compared to the uptake of NP capped with APTMS (1.02%) and BSA (0.86%). Such prominent differences in the levels of NP uptake is likely to be correlated with the explicit mechanisms of interaction between the cells and NP, including the internalisation routes the NP follow, as well as the intracellular processing.

There are several possible entry routes of NP into HepG2 (Figure 5), including macropinocytosis and endocytosis. Individual pathways of this complex machinery can be blocked or inhibited with carefully chosen drugs, introduced at non-lethal doses prior to administration of NP, to interfere with their uptake and intracellular processing,<sup>13</sup> an approach commonly used in virology.<sup>19</sup>

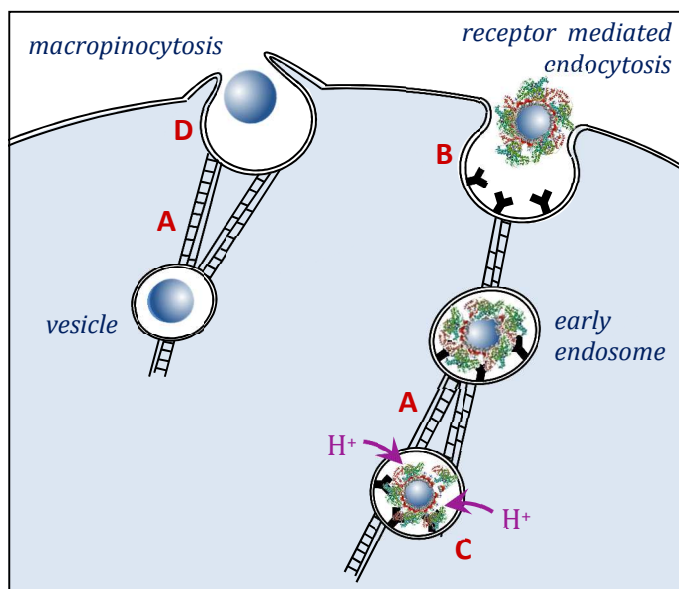


**Figure 5.** Schematic representation of possible cell entry routes and intracellular fate of ZnO NP in HepG2. The following pathways can be disrupted with carefully chosen inhibitors: microtubules and endosome trafficking (A; nocodazole), clathrin mediated endocytosis (B; chlorpromazine), endosome acidification (C; chloroquine) and macropinocytosis (D; benzamil).

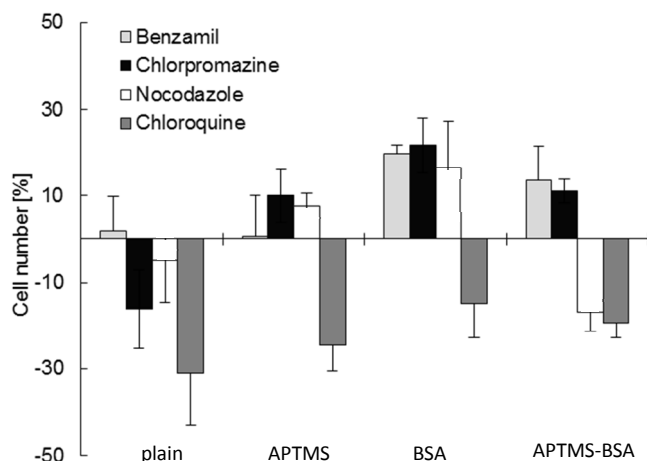


**Figure 6.** Inhibition of ZnO NP uptake by HepG2 with selected drugs (average  $\pm$  stdev,  $n=3$ ).

**Table 3.** Percentage change in the uptake of ZnO NP by HepG2, following pre-treatment with inhibitory drugs (% change compared to non-drug treated controls).

Inhibitor	% Change in NP Uptake			
	plain	ATPMS	BSA	APTMS-BSA
Benzamil	91 $\pm$ 3.6	99 $\pm$ 4.2	67 $\pm$ 2.7	34 $\pm$ 2.7
Chlorpromazine	125 $\pm$ 2.5	86 $\pm$ 4.3	72 $\pm$ 2.2	34 $\pm$ 2.1
Nocodazole	113 $\pm$ 5.6	92 $\pm$ 3.7	65 $\pm$ 3.3	130 $\pm$ 6.5
Chloroquine	124 $\pm$ 5.0	161 $\pm$ 8.4	115 $\pm$ 2.3	142 $\pm$ 5.7

**Figure 6** shows the difference in cell number (derived from label free impedance measurements and representative of cell viability), after treatment with selected uptake inhibiting drugs prior to exposure to NP, as a percentage change from controls treated with NP but without the inhibitors. **Table 3** shows the percentage inhibition of NP uptake by the cells compared to non-drug treated controls as determined by ICP-MS. Pre-incubation of cells with benzamil, an inhibitor of macropinocytosis, lead to an increase in the viability of cells following exposure to NP capped with BSA and APTMS-BSA (as shown by an increase in cell number) and a corresponding decrease in NP internalisation (-33% and -66%, respectively) indicating that this is a likely mechanism of their uptake. This is in agreement with a study showing that inhibition of macropinocytosis and clathrin-mediated endocytosis reduce the uptake of fluorescently labelled albumin<sup>20</sup> and indicate that the surface modification of ZnO NP directly influence their uptake by the cells. No change in cell viability was measured following exposure to plain and APTMS capped NP, indicating that this is not their likely uptake mechanism. Reduction in toxicity and internalisation of APTMS, BSA and APTMS-BSA NP following treatment with chlorpromazine, an inhibitor of clathrin-mediated endocytosis, suggests that clathrin is involved in their uptake. This indicates the most likely uptake mechanism of APTMS capped NP and suggests that BSA and APTMS-BSA NP are taken up by more than one mechanism, indicating that albumin triggers an additional uptake mechanism.

Pre-incubation of cells with nocodazole, and inhibitor of endosome trafficking, lead to an increase in viability following exposure to NP capped with APTMS and BSA, indicating that the endosome trafficking plays an important role in the intracellular fate of these two materials and that the cellular processing of NP is linked to their toxicity. There was also a corresponding reduction in internalisation of the APTMS (-8%) and BSA (-35%) NP as determined by ICP-MS. This suggests that following uptake these NP are encapsulated in membrane-bound endosome vesicles which deliver the NP for sorting and packaging within the cells, a process which also allows the NP to exert a toxic effect upon the cells once they are internalised.

In comparison, pre-incubation of the cells with chloroquine, an inhibitor of endosome acidification, lead to a decrease in cell viability following exposure to all test materials and an increase in NP uptake of between 15-61%. It indicates that this process is involved in cellular mechanism of dealing with toxins. It is suggested that as a defence mechanism, the cells activate endosome acidification machinery to dissolve NP and to allow easier transport and recycling to the extracellular milieu than ZnO in its particulate form. Locked in a particulate form ZnO was shown to be more toxic to cells than when dissolved as ions, because of a different mechanism of action and systemic pathways activation by the particulate matter.<sup>18</sup>

None of the drugs used increased the viability of cells exposed to plain ZnO NP, indicating that macropinocytosis and receptor mediated endocytosis are not their likely uptake mechanisms, pointing towards receptor independent

endocytosis as possible internalisation route of this material, since HepG2 used in this study do not express caveolae.<sup>21</sup>

## Conclusions

Commercial strategies aiming to fully utilise the unique characteristics of NP are increasingly implementing approaches involving NP capping with ligands to reduce their potential toxicity. However, testing the effect of NP surface modifications on the bioactivity of coated NP is challenging and often requires NP characterisation in the presence of a complex test matrix. In this study we apply a label-free approach to study how different NP surface modifications influence their behaviour in biological matrix as well as cellular toxicity and demonstrate how the ligand exchange process can influence NP uptake rate and processing by the cells. Of particular importance in this study is the use of kinetic response measurements that not only allow the NP toxicity profiles to be monitored over time, but also permit more comprehensive investigation of NP interactions with cells, ascertained through inhibition of selected cellular processes. Taken together the data presented in this study highlights that carefully selected and thorough physicochemical and biological *in vitro* characterisation techniques could be used to assess fine differences in potentially adverse effects NP may cause, offering possibility to influence future commercial strategies for NP surface engineering during product development.

## Acknowledgements

Funding from the UK National Measurement Office is gratefully acknowledged. The authors would also like to thank Milena Quaglia from LGC Limited for analysis of the tryptic digests, as well as Anton Page and Patricia Goggin from Biomedical Imaging Unit in Southampton for technical support with TEM imaging.

## Notes and references

<sup>a</sup> LGC Limited, Queens Road, Teddington, TW11 0LY, UK

\* e-mail: damian.marshall@ct.catapult.org.uk

- X. W. Sun and H. S. Kwok, *J. Appl. Phys.*, 1999, **86**, 408-411; H. Cao, J. Y. Xu, D. Z. Zhang, S.-H. Chang, S. T. Ho, E. W. Seelig, X. Liu and R. P. H. Chang, *Phys. Rev. Lett.*, 2000, **84**, 5584-5587.
- E. Koushki, A. Farzaneh and M. H. Majles Ara, *Optik*, 2014, **125**, 220-223; M. K. Debanath and S. Karmakar, *Mat. Lett.*, 2013, **111**, 116-119.
- C. L. Carnes and K. J. Klabunde, *Langmuir*, 2000, **16**, 3764-3772.
- V. Srikant and D. R. Clarke, *Appl. Phys. Lett.* 1997, **70**, 2230-2232.
- M. J. Osmond and M. J. McCall, *Nanotoxicology*, 2010, **4**, 15-41; M. R. Wiesner, G. V. Lowry, P. Alvarez, D. Dionysiou and P. Biswas, *Environ. Sci. Technol.*, 2006, **40**, 4336-4345.
- H. Yin, P. S. Casey, M. J. McCall and M. Fenech, *Langmuir*, 2010, **26**, 15399-15408; N. Lewinski, V. Colvin and R. Drezek, *Small*, 2008, **4**, 26-49; B. Pelaz, S. Jaber, D. J. de Aberasturi, V. Wulf, T. Aida, J. M. de la Fuente, J. Feldmann, H. E. Gaub, L. Josephson, C. R. Kagan, N. A. Kotov, L. M. Liz-Marzán, H. Mattoussi, P. Mulvaney, C. B. Murray, A. L. Rogach, P. S. Weiss, I. Willner and W. J. Parak, *ACS Nano*, 2012, **6**, 8468-8483; A. M. Smith, H. Duan, M. N. Rhyner, G. Ruan and S. Nie, *Phys. Chem. Chem. Phys.*, 2006, **8**, 3895-3903; C. M. Goodman, C. D. McCusker, T. Yilmaz and V. M. Rotello, *Bioconjugate Chem.*, 2004, **15**, 897-900; A. Verma and F. Stellacci, *Small*, 2010, **6**, 12-21.
- F. Grasset, N. Saito, D. Li, D. Park, I. Sakaguchi, N. Ohashi, H. Haneda, T. Roisnel, S. Mornet and E. Duguet, *J. Alloy. Compd.*, 2003, **360**, 298-311; S. George, S. Pokhrel, T. Xia, B. Gilbert, Z. Ji, M. Schowalter, A. Rosenauer, R. Damoiseaux, K. A. Bradley, L. Mädler and A. E. Nel, *ACS Nano*, 2010, **4**, 15-29; P. Kumar, P. Kumar, A. Deep and L. M. Bharadwaj, *Appl. Nanosci.*, 2013, **3**, 141-144.
- G. Maiorano, S. Sabella, B. Sorce, V. Brunetti, M. A. Malvindi, R. Cingolani and P. P. Pompa, *ACS Nano*, 2010, **4**, 7481-7491.
- A. Kroll, M. H. Pillukat, D. Hahn, J. Schnekenburger, *Arch. Toxicol.*, 2012, **86**, 1123-1136; A. M. Horst, R. Vukanti, J. H. Priester and P. A. Holden, *Small*, 2013, **9**, 1753-1764.
- A. E. Nel, L. Madler, D. Velegol, T. Xia, E. M. V. Hoek, P. Somasundaran, F. Klaessig, V. Castranova and M. Thompson, *Nat. Mater.*, 2009, **8**, 543-557; D. Walczyk, F. B. Bombelli, M. P. Monopoli, I. Lynch and K. A. Dawson, *J. Am. Chem. Soc.*, 2010, **132**, 5761-5768; R. Vajtai, Z. A. Lewicka and V. L. Colvin, *Nanomaterial Toxicity, Hazards, and Safety*. In *Springer Handbook of Nanomaterials*, Springer Berlin Heidelberg, 2013, 1117-1142.
- J. M. Seiffert, M.-O. Baradez, V. Nischwitz, T. Lekishvili, H. Goenaga-Infante and D. Marshall, *Chem. Res. Toxicol.*, 2012, **25**, 140-152.
- D. Bartczak, M.-O. Baradez, S. Merson, H. Goenaga-Infante and D. Marshall, *J. Phys.: Conf. Ser.*, 2013, **429**, 012015.
- H. Gao, Z. Yang, S. Zhang, S. Cao, S. Shen, Z. Pang and X. Jiang, *Sci. Rep.*, 2013, **3**, 2534.
- C. Sayes and D. Werheit, *Nanomed. Nanobiotechnol.*, 2009, **1**, 660-670.
- Z. Wang, X. Xie, S. Xiao and J. Liu, *Hydrometallurgy*, 2010, **102**, 87-90.
- F. Geng, K. Song, J. Z. Xing, C. Yuan, S. Yan, Q. Yang, J. Chen and B. Kong, *Nanotechnology*, 2011, **22**, 285101.
- C. Goodman, C. McCusker, T. Yilmaz and V. Rotello, *Bioconjugate Chem.*, 2004, **15**, 897-900; N. Schaeublin, L. Braydich-Stolle, A. Schrand, J. Miller, J. Hutchison, J. Schlager and S. Hussain, *Nanoscale*, 2011, **3**, 410-420.
- C. Hanley, A. Thurber, C. Hanna, A. Punnoose, J. Zhang and D. G. Wingett, *Nanoscale Res. Lett.*, 2009, **4**, 1409-1420; V. Sharm, D. Anderson and A. Dhawan, *Apoptosis*, 2012, **17**, 852-870; S. J. Park, Y. C. Park, S. W. Lee, M. S. Jeong, K.-N. Yu, H. Jung, J.-K. Lee, J. S. Ki and M.-H. Cho, *Toxicol. Lett.*, 2011, **207**, 197-203; P. J. Moos, K. Chung, D. Woessner, M. Honegger, N. S. Cutler and J. M. Veranth, *Chem. Res. Toxicol.*, 2010, **23**, 733-739.
- A. D. Stuart and T. D. K. Brown, *J. Virol.*, 2006, **80**, 7500-7509.
- R. Yumoto, S. Suzuka, K. Oda, J. Nagai and M. Takano, *Drug Metab. Pharmacokinetics*, 2012, **27**, 336-343.
- T. Fujimoto, H. Kogo, R. Nomura and T. Ue, *J. Cell Sci.*, 2000, **113**, 3509-3517; Y. Fu, A. Hoang, G. Escher, R. G. Parton, Z. Krozowski and D. Sviridov, *J. Biol. Chem.*, 2004, **279**, 14140-14146.